Use of Nanotechnology in Remediation of Radionuclides and Heavy Metals

Frank (Fengxiang) X. Han

Dept. of Chemistry and Biochemistry
Jackson State University

Global Perspective

of Pollution by Heavy Metals/Trace Elements

Driving Force

- Global Population Increase and Civilization
  (6.91 billion, by 1.1% in 2009)

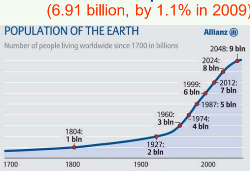

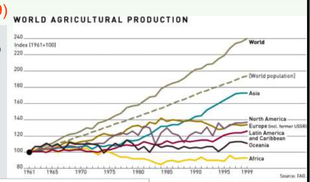

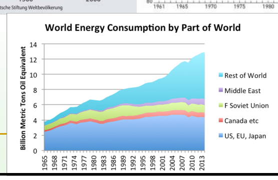

How is the Earth Surface polluted by Heavy Metals/Trace Elements?

Heavy Metal/Trace Element Production

= ?

Pollution

GlobalAnnual Production of Zn, Pb, Cu, Cr, Ni, and Cd since Industrial Age

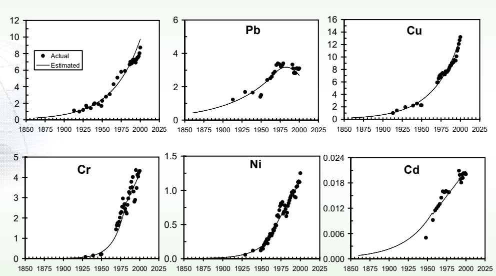

Cumulative Production of Zn, Pb, Cu, Cr, Ni, and Cd since Industrial Age

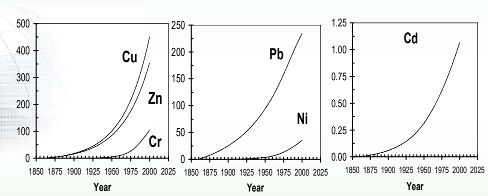

Annual production of As since Industrial Age since Industrial Age

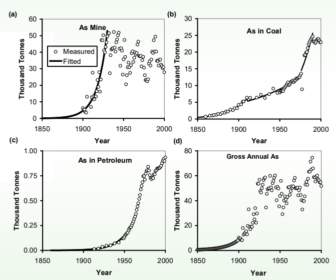

Gross As Production, As Production from Petroleum and Coal since Industrial Age

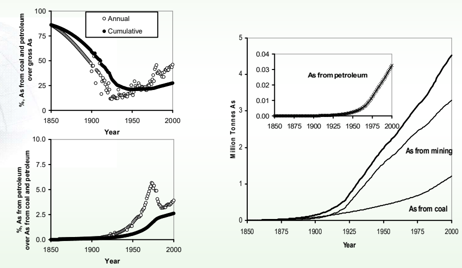

Annual and Cumulative Hg Production

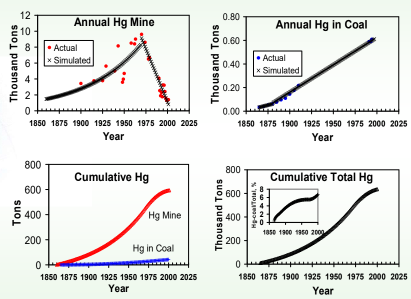

Potential Cumulative Anthropogenic Inputs to Global Arable Soil (0-10 cm)

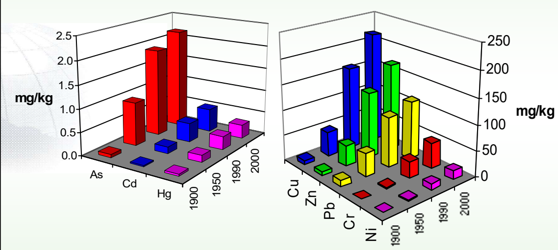

Compared to Global Soil and Lithosphere

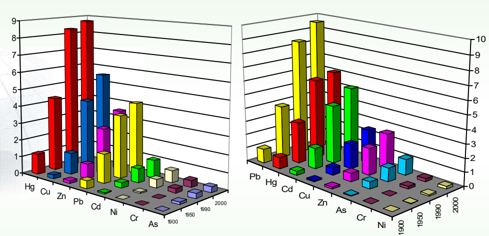

Ratios of Anthropogenic Cumulative Input /World Soil

Ratios of Anthropogenic Cumulative Input /Lithosphere

Global Metal Burden per Capita

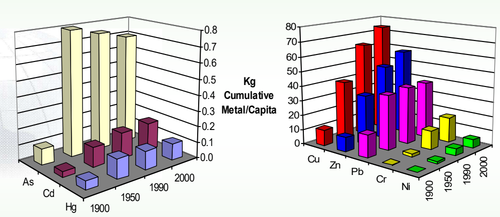

Global Nuclear Radionuclide Pollution

Nuclear Energy

- With the fast growth of global population, the world consumption of energy has been continuously increasing at an annual rate of 2-3%. Fossil fuel energy is the major source of current global energy consumption (37% petroleum, 25% coal and 22% natural gas)
- Due to increasing cost of fuel energy supplies and global warming, nuclear energy has become a promising emission-free clean energy. Currently, nuclear energy accounts for 6% and 8% of the total energy consumption in the world and the U.S., respectively

Nuclear Power Plant Accidents

- 99 nuclear power plant accidents worldwide
- 4 major accidents including the most recent Fukushima Daiichi nuclear disaster (2011), Chernobyl disaster (1986), Three Mile Island accident (1979), and the SL-1 accident (1961).
- Chernobyl: 137Cs, 90Sr, 238Pu and 241Am
- Fukushima Daiichi: 134Cs, 137Cs, 60Co and 131I
- On the other hand, radionuclides were in colloids of groundwater of nuclear ground detonation sites such as the Nevada Test Site. Dissolved organic carbon mobilized actinides (Am, Pu, Np and U) in the groundwater of these sites.

Developing Novel Nanomaterials for Removing Radionuclides and Heavy Metals from Water

To functionalize meso silica for adsorption of Cs, Co, and Sr in contaminated water

MCM-41 (Mobil Composition of Matter No. 41) is a mesoporous alumosilicate with a hierarchical structure.

- Characterization

Particle Size and Zeta Potential
FTIR and Raman Spectroscopy
TEM Images

Adsorption of Cs, Sr, and Co on thiol-functionalized MCM-41

Prepare a mix solution of $CsNO_3$, $Sr(NO_3)_2$, and $Co(NO_3)_2$ at serial concentrations. Add sorbents, shake and filter supernatant. Inductively coupled plasma-mass spectrometry (ICP-MS) was applied.

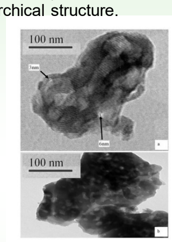

TEM pictures of MCM-41-SH (a and b). The pore sizes were indicated as arrows, measured as 3 nm or 6 nm.

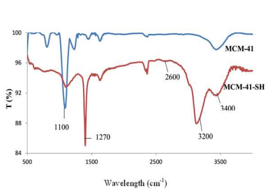

FTIR spectra of MCM-41-SH and MCM-41. The weak peak around 2600 cm-1 indicated the presence of the SH group

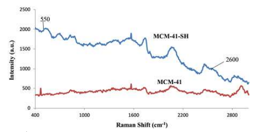

Raman spectra of MCM-41 and MCM-41-SH. Aliphatic carbon chains appeared from 600 cm-1 to 1300 cm-1; the peak around 2600cm-1 confirmed the existence of –SH function group.

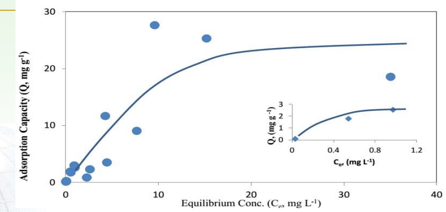

Cs adsorption isotherm from water on MCM-41-SH

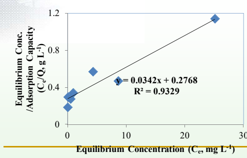

Langmuir model of Cs adsorption from water on MCM-41-SH

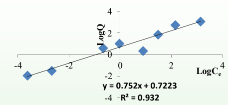

Freundlich model of Cs adsorption from water on MCM-41-SH

Table 1 Comparison of adsorption of Cs on MCM-41-SH as described with Langmuir and Freundlich models

Langmuir Model		Freundlich Model	
R^2	0.93	R^2	0.93
b, L mg^{-1}	0.12	n	1.33
Q, mg g^{-1}	29.24	K_f	5.28

This study indicated that commercially available MCM-41 after being functionalized became more selective on Cs, one of elements with the most difficult to remove. For the next stage study, I consider to make sorbent recyclable.

Developing meso-silica templated nano carbon for removing Cs

- Mesosilica has been used as a stable template to synthesize mesoporous carbon with various functional groups such as hydroxyl, carboxyl, and carbonyl groups, etc.
- Carbon Precursor
  - Ferulic acid, as the carbon precursor, was used for the adsorption of Cs(I) and other several major nuclides such as Co(II) and Sr(II).
  - Ascorbic acid as C precursor and binding to nano magnetite Fe_3O_4, for removing Hg(II) and Pb(II).

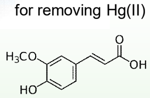

Ferulic acid

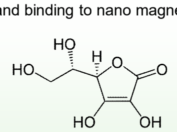

Ascorbic acid

- **Characterization**

TEM, FTIR, and BET are applied to illustrate functional groups and pore structure.

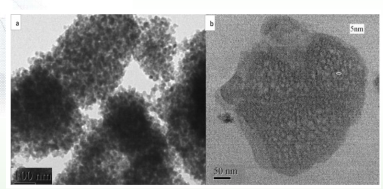

TEM images of ferulic acid-NC (a) and ascorbic acid-NC (b).

FTIR

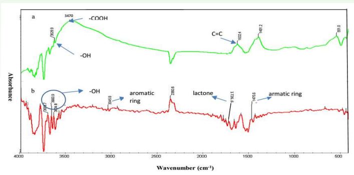

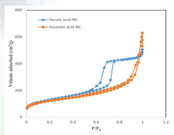

FTIR spectra of ferulic acid-NC (a) and ascorbic acid-NC (b) (upper figure) and BET isotherm of two nano carbons (lower left). Magnetic effect after a permanent magnet was applied to the ascorbic acid-NC (lower right).

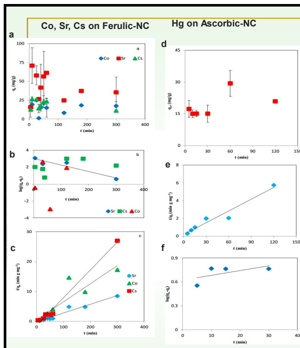

Kinetic study of Co, Sr, and Cs with 0.3 g/L ferulic acid-NC at 25℃ with pH=6~7. Kinetic data (a), pseudo-first order (b), and pseudo-second order (c) were shown. All three elements fit pseudo-second order well.

Kinetic study of Hg with 0.3 g/L ascorbic acid-NC at 25℃ with pH=6~7. Kinetic data (d), pseudo-second order (e), and pseudo-first order (f) were shown.

Adsorption Kinetics

Adsorption Isotherms of Co, Sr and Cs: Phase I and II

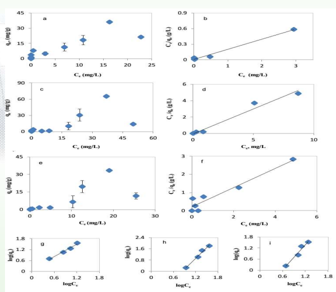

Adsorption isotherms of Co (a), Sr(c), and Cs(e) with 0.3 g/L ferulic acid-NC at 25℃ with pH=6~7:

Langmuir model of Co(b), Sr(d), and Cs(f) for Phase I;

Freundlich model of Co(g), Sr(h), and Cs(i) for Phase II.

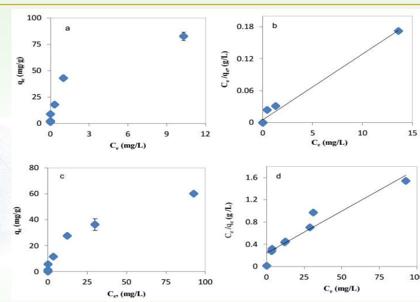

Adsorption isotherm of Hg(a) and Pb(c), with 0.3 g/L ascorbic acid-NC, at 25℃, with pH=6~7: Langmuir model of Hg(b) and Pb(d).

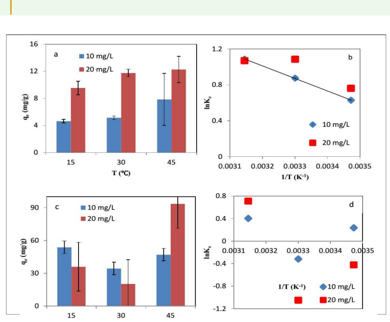

Thermodynamic study of Hg(a) and Pb(c) on ascorbic-NC. Van't Hoff model linear plot was applied to Hg(b) and Pb(d).

Table 3 Thermodynamic parameters of Hg and Pb at 10 and 20 mg/L, on ascorbic acid-NC with 0.3 g/L at pH~6,7.

Metals	Temperature	Initial Concentrations of metals									
	°C	10 mg/L					20 mg/L				
		ΔG (kJ mol⁻¹)	lnK_C	ΔH (kJ mol⁻¹)	ΔS (J mol⁻¹ K⁻¹)	R^2	ΔG (kJ mol⁻¹)	lnK_C	ΔH (kJ mol⁻¹)	ΔS (J mol⁻¹ K⁻¹)	R^2
Hg	15	-1.51	0.63			1	-1.83	0.76			0.74
	30	-2.1	0.88	11.6	45.6		-2.73	1.09	7.93	34.3	
	45	-2.6	1.09				-2.83	1.07			
Pb	15	-0.57	0.24			0.037	1.01	-0.42			0.38
	30	0.8	-0.32				2.64	-1.05			
	45	-1.07	0.4				-1.88	0.71			

-Δ G and + ΔH indicates spontaneous adsorption process; + ΔH indicates endothermic adsorption process

Adsorption of Cs using magnetic heteroatom-functionalized calixarene complex

Calixarene is a building block material in the macrocyclic molecular group. Its unique character was the three-dimensional pre-organization, making it a potential candidate of receptor to many cations and anions, which exhibited potentials for the treatment of nuclear wastewater.

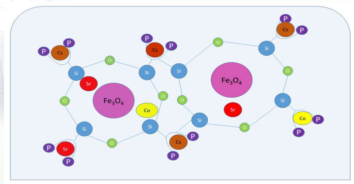

The present study is to synthesize the stable and efficient magnetic calixarene composite for the treatment of Co2+, Sr2+, and Cs+. Two types of commercially available upper-rim sulfur or phosphorous functionalized calixarene were applied and compared. Meso-silica as the anchor was applied to connect the Fe_3O_4 part and the calixarene part.

- **Experiment**

  Synthesis

Characterization
TEM, FTIR, SEM, XRD, BET methods will be applied to elucidate the unique structure of the calix complex.
Adsorption
Cs (from 0 to 2000 mg/L) and Sr solution were prepared.
To examine any competitive behavior with other heavy metals, mix solutions of Sr, Co, Cd, Hg, and Pb from 0 to 2000 mg/L.

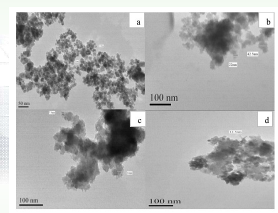

TEM images of Fe_3O_4 NP (a), Si-MN (b), S-Si-MN (c), and P-Si-MN(d).

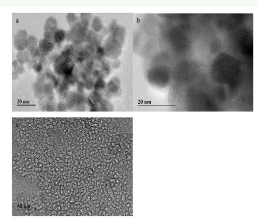

High resolution TEM pictures showed S-Si-MN (a), P-Si-MN (b), and Si-MN (c).

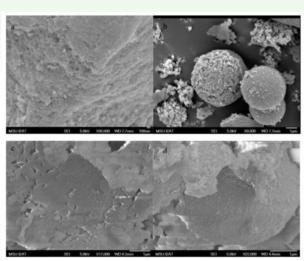

SEM results of P-Si-MN (a&b) and S-Si-MN (c&d).

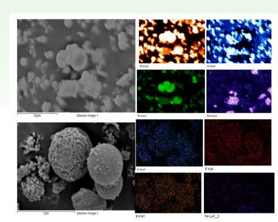

	P S MN				S S MN			
	O	Si	P	Fe	O	Si	S	Fe
We gh %	29.98	26.65	26.83	16.54	40.47	32.77	7.01	19.75
A om c %	47.02	23.82	21.73	7.43	59.26	27.33	5.12	8.29

Energy Dispersive Spectroscopy (EDS) analysis showed the elemental mapping of each composite. On the top is the SEM image of S-Si-MN, and the corresponding elemental mapping results are on the right. The brighter the color, the higher percentage of the element is in that zone. On the bottom are the SEM image of P-Si-MN and the elemental mapping.

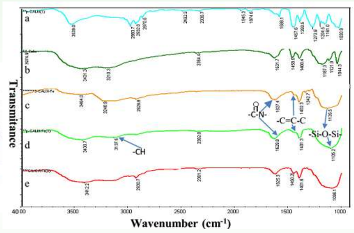

FTIR spectra of phosphoryl group calixarene (a), sulfonic group calixarene (b), S-Si-MN (c), P-Si-MN (d), and Si-MN (e).

Cs Adsorption in Cs Alone System

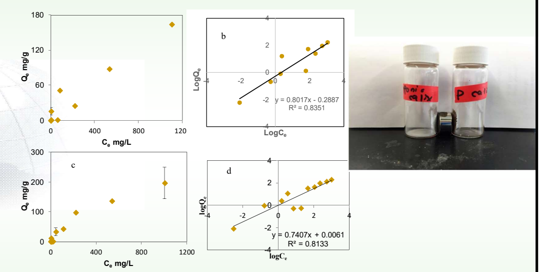

Adsorption of Cs on S-Si-MN. (a) Isotherm; (b) Freundlich model and P-Si-MN (c) isotherm; (d) Freundlich model.

Far right shows magnetic separation

Sr Adsorption in Sr Alone System

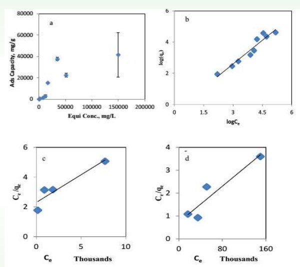

In the individual system, the adsorption of Sr on P-Si-MN. (a) isotherm; (b) Freundlich model; (c) Langmuir model on Phase I; (d) Langmuir model on Phase II.

Co Adsorption in Multimetal system

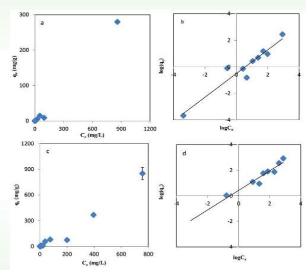

In the multi-cation system, the adsorption isotherm of Co on S-Si-MN (a) and P-Si-MN (c); Freundlich model from S-Si-MN (b) and P-Si-MN (d).

Sr Adsorption in a Multimetal System

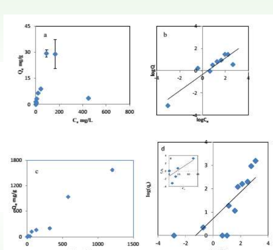

In the multi-cation system, the adsorption of Sr on S-Si-MN (a) isotherm & (b) Freundlich model; on P-Si-MN (c) isotherm & (d) Freundlich model. The inlet of Fig. d showed the Langmuir model of Phase I.

Cd Adsorption in a Multimetal System

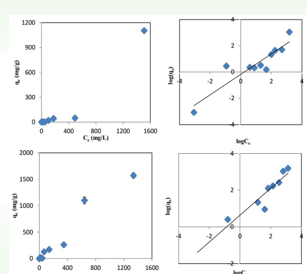

In the multi-cation system, the adsorption isotherm of Cd on S-Si-MN (a) and P-Si-MN (c); Freundlich model from S-Si-MN (b) and P-Si-MN (d).

Hg Adsorption in a Multimetal System

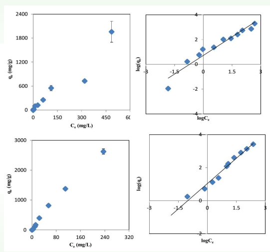

In the multi-cation system, the adsorption isotherm of Hg on S-Si-MN (a) and P-Si-MN (c); Freundlich model from S-Si-MN (b) and P-Si-MN (d).

Pb Adsorption in a Multimetal System

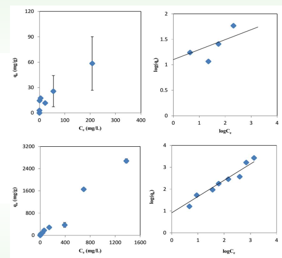

In the multi-cation system, the adsorption isotherm of Pb on S-Si-MN (a) and P-Si-MN (c); Freundlich model from S-Si-MN (b) and P-Si-MN (d).

Comparison of Adsorption Capacity

Adsorbents	Adsorbates	pH	Maximum adsorption capacity (mg/g)	References
am nated graphene ox de NP	Co		116.35	Fang et al., 2014
Graphene ox de hydroxyapat te NP	Sr	2-4	702.18	Wen et al., 2014
Graphene ox de comp exed	Cs		184.74	Sun et al., 2013
w th n trogene and oxygene groups	Sr		147.20	
P S MN	Co Sr Cs	6-7	900 30000 200	**This study**

Other Soil Remediation in my group

- Phytoremediation
- Bioremediation
- Electronic Kinetic Remediation
- Coupled Electronic Kinetic-Phytoremediation
- Soil Washing
- Coupled Electronic Kinetic-Soil Washing

Conclusion

Our lab developed a series of promising meso/nanomaterials for cleaning up Cs, Sr, Co and other radionuclides as well as heavy metals (Cd, Hg, Pb) in contaminated water.

This study shows the promise of novel meso/nanomaterials in removing common radionuclides and heavy metals and provides alternative solutions for water pollution from nuclear industry development.

Acknowledgement

- This study was supported by the U.S. Nuclear Regulatory Commission (NRC-HQ-84-15-G-0042 and NRC–HQ-12-G-38-0038).

Recent Publications

- Meng, et al. 2017. Removing uranium (VI) from aqueous solution with insoluble humic acid derived from leonardite. ***Journal of Environmental Radioactivity*** 180 (2017) 1-8
- Mao, et al. 2017. Effects of operation variables and electro-kinetic field on soil washing of arsenic and cesium with potassium phosphate. ***Water Air and Soil Pollution*** 228: 15. doi:10.1007/s11270-016-3199-y
- Guo, et al. 2016. Development of novel nanomaterials for remediation of heavy metals and radionuclides in contaminated water. ***Nanotechnology for Environmental Engineering*** (Springer). 1:7
- Mao, et al.. 2016. The distribution and elevated solubility of lead, arsenic and cesium in contaminated paddy soil enhanced with the electro-kinetic field. ***International of Journal of Environmental Science and Technology*** 13: 1641–1652.
- Mao, et al. 2016. Remediation of lead, arsenic, and cesium contaminated soil using consecutive washing enhanced with electro-kinetic field. ***Journal of Soils and Sediments***, 10: 2344-2353.
- Billa, et al. 2016. Radioactivity Studies on Farm Raised and Wild Catfish Collected in the Vicinity of a Nuclear Power Plant. ***Journal of Radioanalytical and Nuclear Chemistry.*** 307: 203-210.
- Lawson et al. 2016. Binding, Speciation and Distribution of Cs, Co and Sr in U.S. Coastal Soil under Saturated and Field Capacity Moisture Regimes. ***Journal of Soils and Sediments*** 16 (2): 497-508.
- Mao, et al. 2016. Electro-kinetic remediation coupled with phytoremediation to remove lead, arsenic and cesium from contaminated paddy soil. ***Ecotoxicology and Environmental Safety,*** 125:16-24.
- Gao, et al. 2015. Adsorption of Cs from water on surface modified MCM-41 mesosilicate. **Water Air and Soil Pollution** 226: 288-297
- **Han**, et al. 2003. Assessment of global industrial-age anthropogenic arsenic contamination. ***Naturwissenschaften*** 90: 395-401.
- **Han** et al. 2002. Industrial age anthropogenic inputs of heavy metals into the pedosphere. ***Naturwissenschaften*** 89: 497-504
- **Han FX.** 2007. *Biogeochemistry of Trace Elements in Arid Environments,* pp ~ 380, Springer.

Thanks!